# The effects of outgassing on the transition between effusive and explosive silicic eruptions

Wim Degruyter, Olivier Bachmann, Alain Burgisser, M. Manga

# The effects of outgassing on the transition between effusive and explosive silicic eruptions

W. Degruyter[a,*], O. Bachmann[b], A. Burgisser[c], M. Manga[a]

[a] *Earth and Planetary Science, University of California, Berkeley, USA*
[b] *Department of Earth and Space Sciences, University of Washington, Seattle, USA*
[c] *Institut des Sciences de la Terre d'Orléans CNRS, Université d'Orléans, France*

**Abstract**

The eruption style of silicic magmas is affected by the loss of gas (outgassing) during ascent. We investigate outgassing using a numerical model for one-dimensional, two-phase, steady flow in a volcanic conduit. By implementing Forchheimer's equation rather than Darcy's equation for outgassing we are able to investigate the relative influence of Darcian and inertial permeability on the transition between effusive and explosive eruptions. These permeabilities are defined by constitutive equations obtained from textural analysis of pyroclasts and determined by bubble number density, throat-bubble size ratio, tortuosity, and roughness. The efficiency of outgassing as a function of these parameters can be quantified by two dimensionless quantities: the Stokes number, the ratio of the response time of the magma and the characteristic time of gas flow, and the Forchheimer number, the ratio of the viscous and inertial forces inside the bubble network. A small Stokes number indicates strong coupling between gas and magma and thus promotes explosive eruption. A large Forchheimer number signifies that gas escape from the bubble network is dominated by inertial effects, which leads to explosive behaviour. To provide context we compare model predictions to the May 18, 1980 Mount St. Helens and the August-September 1997 Soufrière Hills eruptions. We show that inertial effects dominate outgassing during both effusive and explosive eruptions, and that in this case the eruptive regime is determined by a new dimensionless quantity defined by the ratio of Stokes and Forchheimer number. Of the considered textural parameters, the bubble number density has the strongest influence on this quantity.

*Corresponding author
*Email address:* wim.degruyter@berkeley.edu (W. Degruyter)

This result has implications for permeability studies and conduit modelling.

*Keywords:* effusive-explosive transition, conduit, textures, permeability, outgassing

## 1. Introduction

The efficiency of gas escape during the ascent of silicic magma governs the transition between effusive and explosive eruptions (Slezin, 1983; Eichelberger et al., 1986; Jaupart and Allegre, 1991; Woods and Koyaguchi, 1994; Slezin, 2003; Gonnermann and Manga, 2007). If the gas can escape readily from the magma, an effusive outpouring of lava occurs. On the other hand, when the gas stays trapped within the ascending magma, it provides the potential energy needed to fragment the magma and produce an explosive eruption. Gas can separate from magma through a network of coalesced bubbles or fractures, both horizontally into the conduit walls and vertically to the surface (Stasiuk et al., 1996; Melnik and Sparks, 1999; Tuffen et al., 2003; Gonnermann and Manga, 2003). Here we study vertical gas segregation through a network of bubbles in order to quantify the effects of permeability on the outcome of an eruption.

Juvenile pyroclasts contain information on the pore-scale geometry of the magma at the time they are quenched. Pyroclasts ejected by Vulcanian eruption, for example, preserve some evidence for the effusive dome-forming phase prior to fragmentation. Formenti and Druitt (2003) found that syn-explosion bubble nucleation may occur, resulting in a uniformly distributed porosity change of $< 15\%$, which suggests that porosity trends with depth are approximately preserved in the pyroclasts. Giachetti et al. (2010) used such pyroclasts to determine pre-explosive conditions of the 1997 eruptions at Soufrière Hills Volcano, Montserrat. Products of Plinian eruptions on the other hand can record the state of the magma at fragmentation provided post-fragmentation deformation is limited. This is true for highly viscous magmas and relatively small pyroclasts. A snapshot of the outgassing history can thus be found in these pyroclasts, and measuring their permeability can provide insights into outgassing (Figure 1; Klug and Cashman, 1996; Melnik and Sparks, 2002a; Rust and Cashman, 2004; Bernard et al., 2007; Takeuchi et al., 2008; Wright et al., 2009; Bouvet de Maisonneuve et al., 2009; Yokoyama and Takeuchi, 2009).

It has been suggested that outgassing during magma ascent can be described by Forchheimer's law (Forchheimer, 1901; Rust and Cashman, 2004), an extension to Darcy's law, which accounts for the effects of turbulence,

$$\left|\frac{dP}{dz}\right| = \underbrace{\frac{\mu_g}{k_1}U}_{\text{viscous term}} + \underbrace{\frac{\rho_g}{k_2}U^2}_{\text{inertial term}}, \quad (1)$$

where $z$ is the direction of flow, $P$ is the pressure, $U$ is the volume flux, $\mu_g$ is the viscosity, $\rho_g$ is the density of the gas phase. The Darcian permeability, $k_1$, and the inertial permeability, $k_2$, account for the influence of the geometry of the network of bubbles preserved in the juvenile pyroclasts. Figure 1 compiles permeability measurements as a function of the connected porosity found in pyroclasts. In general, permeability increases with increasing porosity, but there is large variability in the data sets. Effusive products are overall less porous than their explosive counterparts, but have a similar range over 5 to 6 orders of magnitude in Darcian and inertial permeability.

Textural studies have shown that the spread of permeability found in juvenile pyroclasts is caused by the variation in size, shape, tortuosity, and roughness of connected channels through the network of bubbles (Figure 1; Blower, 2001; Bernard et al., 2007; Wright et al., 2006, 2009; Degruyter et al., 2010a,b). Several constitutive equations that link these parameters to the Darcian and inertial permeability have been proposed. In the present study we use the Kozeny-Carman or equivalent channel equations as discussed by Degruyter et al. (2010a)

$$k_1 = \frac{r_t^2}{8}\phi_c^m, \quad (2)$$

$$k_2 = \frac{r_t}{f_0}\phi_c^{\frac{1+3m}{2}}, \quad (3)$$

with $\phi_c$ the connected porosity, $r_t$ the throat radius (the minimum cross section between two coalesced bubbles). The parameter $m$ is the tortuosity or cementation factor connected to the tortuosity $\tau$ using Archie's law,

$$\tau^2 = \phi_c^{1-m}, \quad (4)$$

with the tortuosity defined as the length of the connected channels divided by the length of the porous medium. The parameter $f_0$ is a fitting constant that only appears in the

expression for $k_2$, which we refer to as the roughness factor. We adapt this formulation for outgassing in a conduit flow model and apply it to two well-studied eruptions: (i) the Plinian phase of the May 18, 1980 eruption of Mount St. Helens, USA (MSH 1980) and (ii) the dome-forming eruptions of August-September 1997 at Soufrière Hills Volcano, Montserrat (SHV 1997). These case studies allow us to understand the implications of using Forchheimer's equation rather than Darcy's equation for outgassing during an eruption. We use scaling to quantify the relative importance of the textural parameters and show where further understanding is needed.

## 2. Model

Conduit flow models have been successful in the past to demonstrate how gas loss determines eruption style (Woods and Koyaguchi, 1994; Melnik and Sparks, 1999; Yoshida and Koyaguchi, 1999; Slezin, 2003; Melnik et al., 2005; Kozono and Koyaguchi, 2009a,b, 2010). We adapt the model from Yoshida and Koyaguchi (1999) and Kozono and Koyaguchi (2009a,b, 2010), which assumes a one-dimensional, steady, two-phase flow in a pipe with constant radius. Relative motion between the magma (melt + crystals) and gas phase is accounted for through interfacial drag forces. The exsolution of volatiles is in equilibrium and the magma fragments when the gas volume fraction reaches a critical value $\phi_f$. We consider fragmentation governed by a critical strain rate (Papale, 1999) and critical overpressure (Zhang, 1999); details are in Appendix B. This changes the flow from a permeable foam to a gas phase with pyroclasts in suspension at which point the magma-gas friction and wall friction forces are adjusted. The model of Kozono and Koyaguchi (2009a) is adapted for our purpose in two ways: (i) the description of the magma rheology, and (ii) the description of the interphase drag force.

The governing equations are:

$$\frac{d(\rho_m u_m(1-\phi))}{dz} = -\frac{dn}{dz}q, \tag{5}$$

$$\frac{d(\rho_g u_g \phi)}{dz} = \frac{dn}{dz}q, \tag{6}$$

$$\rho_m u_m(1-\phi)\frac{du_m}{dz} = -(1-\phi)\frac{dP}{dz} - \rho_m(1-\phi)g + F_{mg} - F_{mw}, \tag{7}$$

$$\rho_g u_g \phi \frac{du_g}{dz} = -\phi\frac{dP}{dz} - \rho_g \phi g - F_{mg} - F_{gw} \tag{8}$$

Equations (5)-(6) represent the conservation of mass and equations (7)-(8) the conservation of momentum for the magma phase ($m$) and the gas phase ($g$), where $z$ is the vertical coordinate, $u$ is the vertical velocity, $\rho$ is the density, $\phi$ is the gas volume fraction, $n$ is the gas mass flux fraction, $q$ is the total mass flux, $P$ is the pressure, $F_{mg}$ is the magma-gas friction, and $F_{mw}$ and $F_{gw}$ are the wall friction with the magma and gas phase respectively. The magma is incompressible and the gas density follows the ideal gas law,

$$\rho_g = \frac{P}{RT}, \tag{9}$$

where $R$ is the specific gas constant of water and $T$ is the temperature. Gas exsolution is governed by Henry's law for water,

$$n = \frac{c_0 - sP^{1/2}}{1 - sP^{1/2}} \quad (n \geq 0), \tag{10}$$

where $s$ is the saturation constant for water, and $c_0$ is the initial (dissolved) water content.

### *2.1. Rheology*

The wall friction is governed by the magma phase below the fragmentation depth. As viscosity exerts a first order control on eruption dynamics, we replace the constant viscosity used in Kozono and Koyaguchi (2009a,b) by a viscosity $\mu_m$ that depends on magma properties

by combining models of Hess and Dingwell (1996) and Costa (2005):

$$F_{mw} = \begin{cases} \frac{8\mu_m u_m}{r_c^2} & \phi \leq \phi_f \\ 0 & \phi > \phi_f \end{cases}, \tag{11}$$

$$\log(\mu) = -3.545 + 0.833\ln(100c) + \frac{9601 - 2368\ln(100c)}{T - (195.7 + 32.25\ln(100c))} \tag{12}$$

$$\theta = \left\{1 - c_1 \mathrm{erf}\left(\frac{\sqrt{\pi}}{2}\chi\left[1 + \frac{c_2}{(1-\chi)^{c_3}}\right]\right)\right\}^{-B/c_1} \tag{13}$$

$$\mu_m = \mu(c, T)\theta(\chi) \tag{14}$$

$r_c$ is the conduit radius, $c = sP^{1/2}$ is the dissolved water mass fraction, $\chi$ is crystal content, $B$ is Einstein's coefficient, and $c_1$, $c_2$, $c_3$ are fitting coefficients. Once magma fragments we use turbulent gas-wall friction,

$$F_{gw} = \begin{cases} 0 & \phi \leq \phi_f \\ \frac{\lambda_w}{4r_c}\rho_g|u_g|u_g & \phi > \phi_f \end{cases} \tag{15}$$

where $\lambda_w$ is a drag coefficient.

### *2.2. Outgassing*

Below the fragmentation depth equation (1) is implemented for the interphase drag force $F_{mg}$; above the fragmentation depth we use the model in Yoshida and Koyaguchi (1999). To ease calculations before and after fragmentation there is a gradual transition region between $\phi_f$ and a slightly higher gas volume fraction that we define as $\phi_t = \phi_f + 0.05$.

$$F_{mg} = \begin{cases} \left(\frac{\mu_g}{k_1} + \frac{\rho_g}{k_2}|u_g - u_m|\right)\phi(1-\phi)(u_g - u_m) & \phi \leq \phi_f \\ \left(\frac{\mu_g}{k_1} + \frac{\rho_g}{k_2}|u_g - u_m|\right)^{1-t}\left(\frac{3C_D}{8r_a}\rho_g|u_g - u_m|\right)^t \phi(1-\phi)(u_g - u_m) & \phi_f < \phi \leq \phi_t \\ \frac{3C_D}{8r_a}\rho_g\phi(1-\phi)|u_g - u_m|(u_g - u_m) & \phi > \phi_t \end{cases}, \tag{16}$$

$$t = \frac{\phi - \phi_t}{\phi_f - \phi_t},$$

where $C_D$ is a drag coefficient and $r_a$ is the average size of the fragmented magma particles. To implement the Kozeny-Carman type equations (2) and (3) we have to make some further assumptions about the network of bubbles:

1. Various critical porosity values for percolation have been cited in the literature (Blower, 2001; Burgisser and Gardner, 2004; Okumura et al., 2006; Namiki and Manga, 2008; Takeuchi et al., 2009; Laumonier et al., 2011) ranging from 0.1 to 0.8 gas volume fraction. Here we assume continuous percolation, i.e. the percolation threshold is zero and the connected porosity is equal to the gas volume fraction ($\phi_c = \phi$). Zero permeability has the same effect as very low permeability as the two phases remain coupled in both cases. We note that varying the tortuosity factor is therefore equivalent as varying the percolation threshold as it controls the rate at which the permeability increases. A high tortuosity factor leads to a longer delay in developing permeability as would a larger percolation threshold.
2. The average throat radius $r_t = f_{tb} r_b$, where $f_{tb}$ is the throat-bubble size ratio and $r_b$ is the average bubble size.
3. The average bubble size is determined from the bubble number density and the gas volume fraction as in Gonnermann and Manga (2005),

$$r_b = \left( \frac{\phi}{\frac{4\pi}{3} N_d (1-\phi)} \right)^{1/3}. \tag{17}$$

These asumptions bring us to the following closure equations for the permeability

$$k_1 = \frac{(f_{tb} r_b)^2}{8} \phi^m, \tag{18}$$

$$k_2 = \frac{(f_{tb} r_b)}{f_0} \phi^{\frac{1+3m}{2}}. \tag{19}$$

Bounds on the four parameters can be found in the literature: $N_d = 10^8$–$10^{16}$ m$^{-3}$ (Klug and Cashman, 1994; Polacci et al., 2006; Sable et al., 2006; Giachetti et al., 2010), $f_{tb} = 0.1 - 1$ (Saar and Manga, 1999; Degruyter et al., 2010a), $m = 1 - 10$ (Le Pennec et al., 2001; Bernard et al., 2007; Wright et al., 2009; Degruyter et al., 2010a,b), and Degruyter et al. (2010a) estimated $f_0$ between 10 and 100 for pumices. For comparison, $f_0$ for permeameter standards used by Rust and Cashman (2004) is estimated to be around 0.025 and for packed beds a value of 1.75 is found (Ergun, 1952).

The set of equations (5)-(19) can be converted into two ordinary differential equations for $P$ and $\phi$. We set the differential velocity between the two phases to be initially zero.

In combination with two boundary conditions: (i) initial pressure $P_0$, and (ii) atmospheric pressure or the choking condition at the vent, this 2-point boundary value problem is solved using the ordinary differential equation solver *ode23s* built in Matlab (Shampine and Reichelt, 1997) in combination with a shooting method. Table 1 summarizes model parameters used in this study.

The behaviour of this model allows us to distinguish between explosive and effusive eruptions. Figure 2 shows profiles of pressure, gas volume fraction, velocity, and permeability for a representative explosive and effusive case. In the explosive case the pressure rapidly decreases just prior to fragmentation, while in the effusive case the pressure remains close to magmastatic (Figure 2a). The gas volume fraction reaches high values in the case of an explosive eruption, while in the effusive case it reaches a maximum and decreases at low pressures (Figure 2b). The velocity of the gas phase starts to differ from that of the magma phase at depth in the case of an effusive eruption, while in the explosive case velocities of both phases are nearly equal until fragmentation after which they start to differ (Figure 2c). Both Darcian and inertial permeability are larger at similar pressures in the case of an effusive eruption compared to the explosive case (Figure 2d).

## 3. Stokes and Forchheimer number

We focus on the influence of the textural parameters $N_d$, $f_{tb}$, $m$, and $f_0$ on the eruption style. We therefore non-dimensionalize the equations (5)-(19) using initial and boundary conditions as reference values to extract dimensionless quantities that depend on textures (see Appendix A for details). These are found to be the Stokes number, St, and the Forchheimer number, Fo. St is the ratio of the response time scale of the magma and the characteristic flow time of the gas phase

$$\mathrm{St} = \frac{\tau_V}{\tau_F} = \frac{\frac{\rho_m k_{10}}{\mu_g}}{\frac{r_c}{U_0}} \tag{20}$$

with $U_0$ and $k_{10}$ the reference velocity and Darcian permeability respectively (Appendix A). When St is small the magma and gas phase are closely coupled and ascend at the same speed, while for a large St the gas decouples from the magma and can ascend more rapidly

than the magma. Fo is the ratio of the inertial term and the viscous term in Forchheimer's equation

$$\mathrm{Fo} = \frac{\rho_{g0} k_{10} U_0}{k_{20} \mu_g}. \tag{21}$$

with $\rho_{g0}$ and $k_{20}$ the reference gas density and inertial permeability respectively (Appendix A). For a low Fo the outgassing is controlled by the Darcian permeability, while for a high Fo the inertial permeability is dominant. We are now able to explore the effusive-explosive transition in terms of St and Fo when conduit geometry and magma properties are held constant. In other words, by looking at specific eruptions we can single out the influence of textures from other parameters. This strategy is used in the following section. Monte Carlo simulations are used to explore the texture parameter space defined by $N_d$, $f_{tb}$, $m$, and $f_0$. We determine if the eruption is explosive or effusive for each combination of parameters and then map the results on the (St,Fo)-space.

## 4. Results

### *4.1. Mount St. Helens May 18, 1980 eruption*

The MSH 1980 eruption is a good case study of an explosive eruption as extensive data has been collected on magma properties, conduit geometry, and textures. We use the magma properties as obtained by Blundy and Cashman (2005) and listed in Table 1. Following Dobran (1992) the conduit length was estimated from lithostatic pressure $P_0/\rho g = 5291$ m for a wall rock density of 2700 kg/m$^3$. The fragmentation criterion is set by a critical gas volume fraction $\phi_f$ at 0.8 as found in the white pumice produced by this eruption (Klug and Cashman, 1994). We use a conduit radius of $r_c = 30$ m to match the mass flow rates estimated by Carey et al. (1990). Figure 2 shows the typical behaviour of an explosive eruption for these conditions.

The results of the Monte Carlo simulations over the texture parameter space are divided into explosive and effusive eruptions and projected on a (St,Fo)-map (Figure 3). Parameters leading to explosive eruptions occupy a region of the (St,Fo)-space separated from the ones of leading to effusive eruptions. The separation between these two regions can be approximated by a linear relationship defined by a critical Stokes number $\mathrm{St}_c$ and critical Forchheimer

number $\mathrm{Fo}_c$,

$$\mathrm{Fo} = \frac{\mathrm{Fo}_c}{\mathrm{St}_c}(\mathrm{St} - \mathrm{St}_c). \tag{22}$$

Such a relationship can be expected when inspecting equation (A.14) that shows that the dimensionless drag is inversely correlated with St and linearly with Fo. For MSH 1980 conditions we found $\mathrm{St}_c \approx 10^{-3}$ and $\mathrm{Fo}_c \approx 50$.

The definition of St and Fo in combination with the effusive-explosive map can now be used to interpret the influence of each of the textural parameters individually (Figure 3a). Starting from an arbitrarily chosen point on the (St,Fo) map, we increase the value of one of the textural parameters, while keeping the others constant. Increasing the bubble number density $N_d$ leads to higher coupling between gas and magma, while turbulent outgassing becomes less dominant. This results in conditions favorable for explosive eruptions. The opposite effect is noted for the throat-bubble ratio $f_{tb}$. An increase of the tortuosity factor $m$ leads to increased coupling between the gas and magma as well as increased dominance of turbulent outgassing, which makes explosive eruptions more likely. Increasing the roughness factor $f_0$ increases Fo and leaves St constant. This brings conditions closer to the explosive regime where outgassing is governed by the inertial term in equation (1). The size of the arrows is based on the variability of each of the parameters found in the literature. The large range in measurements of bubble number density implies that this is the main textural feature that controls outgassing. The influence of other parameters is smaller, but we note that uncertainty can be large, especially in the case of the roughness factor $f_0$ for which data are sparse.

The textural studies by Klug and Cashman (1994, 1996) provide constraints on where the MSH 1980 eruption falls on this regime diagram (Figure 3b). A bubble number density of $N_d = 10^{15}$ m$^{-3}$ and tortuosity factor of $m = 3.5$ was measured. The St and Fo number range for the MSH 1980 eruption (Figure 3b) predict a permeability between $5 \times 10^{-14}$ m$^2$ and $5 \times 10^{-12}$ m$^2$ near fragmentation in agreement with the data of Klug and Cashman (1996). The failure of the bubbles to form larger connected channels does not allow for the gas to decouple from the magma and an explosive eruption results ($\mathrm{St} < \mathrm{St}_c$). The spread for the roughness factor $f_0$ puts the MSH 1980 eruption in the turbulent outgassing

regime ($\mathrm{Fo} > \mathrm{Fo}_c$), implying that the outgassing was dominated by the inertial permeability. Measurements of inertial permeability on MSH 1980 pyroclasts could test this hypothesis.

The use of a critical gas volume fraction as a criterion for fragmentation has been shown to be oversimplified and a stress-based criterion either by critical strain rate or gas overpressure is now favored (Dingwell, 1996; Papale, 1999; Zhang, 1999). However, using different fragmentation mechanisms in a one-dimensional conduit model leads to qualitatively similar results as the runaway effect that leads to increased acceleration will ensure all fragmentation criteria will be met over the same narrow depth interval (Melnik and Sparks, 2002b; Massol and Koyaguchi, 2005). In other words, a critical gas volume fraction has similar consequences as a critical strain rate or overpressure in this type of model. This effect is demonstrated here using a criterion based on strain rate and one on overpressure (Appendix B). The strain rate criterion leads to explosive eruptions at a gas volume fraction of about 0.85, while the overpressure criterion was equivalent to a gas volume fraction near 0.6. This leads to a shift in the critical Stokes number defining the transition curve, while its shape is preserved (Figure 3b). We have chosen the critical gas volume fraction that matches the observations in the pyroclasts of the MSH 1980 and note that this is equivalent to the choice of a critical stress criterion.

The calculated mass flow rates vary little within each of the eruption regimes, showing that textural parameters have little influence on it. Rather, mass flow rate appears dominantly controlled by the magma properties and conduit geometry in combination with the imposed boundary conditions at the top and bottom of the conduit. In the explosive regime the mass flow rate is limited by the choked flow condition at the vent and the conduit radius. For the MSH 1980 conditions we obtain $2 \times 10^7$ kg/s by setting the conduit radius to match the mass flow rate estimates of Carey et al. (1990). In the effusive regime the top boundary condition becomes the ambient pressure and mass flow rates are controlled mostly by magma viscosity and conduit radius (Melnik et al., 2005; Kozono and Koyaguchi, 2009a,b). For the MSH 1980 conditions we find a mass flow rate around $2 \times 10^6$ kg/s, an order of magnitude smaller than in the explosive case. The lava dome growth that followed the MSH 1980 eruption had mass flow rates around $1 - 5 \times 10^4$ kg/s (Moore et al., 1981).

This large mismatch implies that the rheology and/or geometry during the dome-forming eruption significantly changed from the explosive MSH 1980 eruption. These issues could be addressed by incorporating improved rheology laws (Cordonnier et al., 2009) as well as crystalllization kinetics (Blundy and Cashman, 2005; Melnik et al., 2011) into the model. However, we can conclude that bubble number density, throat-bubble size ratio, tortuosity, and roughness factor play a secondary role in controlling the mass flow rate.

### *4.2. August-September 1997 Soufrière Hills Volcano dome-forming eruptions*

The SHV 1997 dome-forming eruptions provide a well-defined case study for an effusive eruption. Note that we use our model only for the dome-forming phase and not for the Vulcanian eruptions, which require a model that contains transient dynamics (Melnik and Sparks, 2002b; de' Michieli Vitturi et al., 2010; Fowler et al., 2010). We used the eruption conditions summarized by Melnik and Sparks (1999) and Clarke et al. (2007): a temperature of 1123 K, conduit length of 5 km, initial pressure of 120 MPa, volatile content of 4.6 wt.% water, and magma density of 2450 kg/m$^3$. As was evident from the simulations under MSH 1980 eruption conditions, in the case of effusive eruptions crystallization due to decompression needs to be taken into account in order to capture the lower mass flow rates. We adopt the parametrization as formulated by de' Michieli Vitturi et al. (2010) based on the work of Couch et al. (2003) for the relationship between $\chi$ and $P$

$$\chi = \min\left[\chi_{\max}, \chi_0 + 0.55\left(0.58815\left(\frac{P}{10^6}\right)^{-0.5226}\right)\right] \tag{23}$$

where $\chi_{\max} = 0.6$ and the initial crystal volume fraction is 0.45. Setting the conduit radius at $r_c = 22.5$ m gives a mass flow rate of $3.5 \times 10^4$ kg/s in the effusive regime, in agreement with Druitt et al. (2002). Figure 2 shows example (effusive) profiles produced for these conditions. The mass flow rate in the explosive regime under SHV 1997 conditions is higher by nearly two orders of magnitude, $2.2 \times 10^6$ kg/s. We stress that this is not related to the mass flow rate associated to the Vulcanian explosions at Soufrière Hills Volcano as we only model steady state eruptions, which are dynamically very different from the Vulcanian eruptions (Melnik and Sparks, 2002b; de' Michieli Vitturi et al., 2010; Fowler et al., 2010).

Using again the strategy of Monte Carlo simulations over the textural parameter space, we obtain a new (St,Fo)-map for SHV 1997 conditions that is split into an effusive and explosive region by a transition curve approximated by equation (22) with $\mathrm{St}_c = 2.5 \times 10^{-5}$ and $\mathrm{Fo}_c = 100$. There is a strong shift of the transition curve compared to MSH 1980 with $\mathrm{St}_c$ about two orders of magnitude smaller. This is due to the two orders of magnitude increase of the effective viscosity controlled by the increase in crystal content during ascent. A parameter that is highly uncertain is the critical condition for explosive eruption, as we cannot interpret pyroclast vesicularity of the SHV 1997 eruption in the same fashion as the quenched samples from MSH 1980 eruption. We have chosen $\phi_f = 0.8$.

The bubble number density of the SHV 1997 eruptions during the dome-forming stage is between $10^9$ and $10^{10}$ $\mathrm{m}^{-3}$, based on the large-bubble population in the pyroclasts produced by the Vulcanian eruptions (Giachetti et al., 2010). The St-Fo region defined by this number is indicated in black on Figure 4a. This region can be refined by using the relationship between pressure and gas volume fraction in the conduit as reconstructed by Clarke et al. (2007) and Burgisser et al. (2010). Using Monte Carlo simulations we can search for the St-Fo values that best fit this profile. There is a large spread of the data near the top of the conduit ($< 10$ MPa) indicating a complex and non-unique behaviour in the conduit plug in between Vulcanian eruptions (de' Michieli Vitturi et al., 2010). Therefore we fit the model to the data at greater depth ($> 10$ MPa). The best fit as determined by the lowest chi-square value was $\mathrm{St} = 2.6 \times 10^{-1}$, $\mathrm{Fo} = 3.7 \times 10^4$, which can be formed by e.g. $N_d = 10^{9.5}$ $\mathrm{m}^{-3}$, $f_{tb} = 10^{-0.5}$, $m = 2.1$, and $f_0 = 10$ (Figure 4b). Below the conduit plug, bubbles create large enough pathways through the magma to allow gas escape at low gas volume fraction, thereby hindering magma acceleration ($\mathrm{St} > \mathrm{St}_c$). Figure 4b indicates, as in the case of MSH 1980, that outgassing is turbulent ($\mathrm{Fo} > \mathrm{Fo}_c$) and dominated by inertial permeability.

### *4.3. Influence of turbulent outgassing on the effusive-explosive transition*

The transition curve separating the effusive and explosive eruption regimes in terms of textures is determined by a critical Stokes and Forchheimer number, the values of which will

depend on magma properties and conduit geometry, i.e.

$$\mathrm{St}_c = \Phi_1 \left(\mathrm{Re}, \mathrm{Fr}, \mathrm{Ma}, c_0, \chi_0, \phi_f, \delta, \sigma, a_r\right), \tag{24}$$

$$\mathrm{Fo}_c = \Phi_2 \left(\mathrm{Re}, \mathrm{Fr}, \mathrm{Ma}, c_0, \chi_0, \phi_f, \delta, \sigma, a_r\right). \tag{25}$$

Regardless of the exact forms of these equations, the results show a change in the eruption dynamics when changing from laminar ($\mathrm{Fo} \ll \mathrm{Fo}_c$) to turbulent outgassing ($\mathrm{Fo} \gg \mathrm{Fo}_c$). This becomes more clear when we inspect equation (22) and rewrite it as

$$\mathrm{St} = \mathrm{St}_c \left(1 + \frac{\mathrm{Fo}}{\mathrm{Fo}_c}\right). \tag{26}$$

We see that in the case of laminar outgassing ($\mathrm{Fo} \ll \mathrm{Fo}_c$) the transition is simply described by $\mathrm{St} \approx \mathrm{St}_c$. In the case of turbulent outgassing ($\mathrm{Fo} \gg \mathrm{Fo}_c$) the transition occurs when

$$\Pi = \frac{\mathrm{St}}{\mathrm{Fo}} = \frac{\rho_m k_{20}}{\rho_{g0} r_c} \approx \Pi_c = \frac{\mathrm{St}_c}{\mathrm{Fo}_c}, \tag{27}$$

with $\Pi$ a new dimensionless quantity defined as the ratio of the St and Fo. Textural measurements on juvenile pyroclasts in combination with our numerical results suggest that $\mathrm{Fo} \gg \mathrm{Fo}_c$ (Figures 3b and 4b) and thus that $\Pi$ is the relevant quantity for the effusive-explosive transition rather than St. Equation (27) reveals that the variation of $\Pi$ is mostly due to the ratio of the characteristic inertial permeability with respect to the conduit radius as the density ratio between the magma and the gas will not vary much over a wide range of parameters. Hence, in order to have an effusive eruption the inertial permeability that has to develop during a volcanic eruption needs to be higher in a conduit with a large radius than one with a small radius. In other words, a conduit with a large radius is more likely to produce an explosive eruption.

## 5. Concluding remarks

We developed a model to study the effect of outgassing on eruption style with a specific focus on the effect of using Forchheimer's equation instead of Darcy's equation. We suggest that the inertial term in Forchheimer's equation is dominant during both explosive and effusive eruptions. In terms of textural parameters, the radius of connected channels through

the bubble network dominates the outgassing dynamics. The channel radii are controlled by bubble number density and throat-bubble size ratio, and can vary over many orders of magnitude. Higher tortuosity and roughness factor increase the chances for an explosive eruption, but are less important. However, attention needs to be drawn towards the roughness factor as it is the least constrained parameter. Even if the roughness factor would be lowered by several orders of magnitude, the estimated Fo for MSH 1980 and SHV 1997 would still be above $Fo_c$. In terms of dimensionless parameters this means that the shift in eruption style is not governed by St as previously assumed (e.g., Melnik et al., 2005; Kozono and Koyaguchi, 2009a,b) but by $\Pi$ as defined in equation (27). This result has implications for (i) permeability studies on juvenile pyroclasts that need to quantify the controls on inertial permeability (Rust and Cashman, 2004; Mueller et al., 2005; Takeuchi et al., 2008; Bouvet de Maisonneuve et al., 2009; Yokoyama and Takeuchi, 2009; Degruyter et al., 2010a) and (ii) conduit models that need to include the inertial term in the closure equation for outgassing (Fowler et al., 2010).

Products from effusive eruptions tend to have a lower porosity than their explosive counterparts, while their permeability can reach similar high values (Figure 1). Although pyroclasts of effusive eruptions can be altered by bubble expansion after dome collapse or bubble collapse during emplacement, the porosity-permeability measurements in combination with the conduit model show that high permeability at low porosity can be explained by a larger radius of permeable channels. Such channels can develop due to low bubble number density (Giachetti et al., 2010) and early coalescence due to pre-eruptive magma heating (Ruprecht and Bachmann, 2010) or deformation (Okumura et al., 2006; Laumonier et al., 2011). Hysteresis, whereby high permeability is preserved and porosity is decreased by bubble collapse, can further enhance the difference between effusive and explosive products (Saar and Manga, 1999; Rust and Cashman, 2004; Michaut et al., 2009).

Several additions to the model can be made to improve quantification of the effusive-explosive transition. The most important include adding spatial (Dufek and Bergantz, 2005) and temporal variations (Melnik and Sparks, 2002b; de' Michieli Vitturi et al., 2010; Fowler et al., 2010) as well as non-equilibrium growth of bubbles (Burgisser and Gardner, 2004;

Gonnermann and Manga, 2005) and crystals (Melnik et al., 2011). In explosive eruptions, delayed bubble growth will reduce development of permeability and crystals will not be able to grow fast enough to increase viscosity and reduce the ascent speed. On the other hand, in effusive eruptions both bubble and crystal growth will be closer to equilibrium. Including spatial and temporal variation will help identify the development of heterogeneity of permeability inside the conduit.

By treating the textural properties independent from magma properties and conduit geometry we were able to distill the relative importance of these properties on outgassing. However, textures are intimately tied to the magma properties as they control nucleation, growth, deformation and coalescence of bubbles. For example, bubble number density will increase with increasing decompression rate (Toramaru, 2006) and decrease due to coalescence (Burgisser and Gardner, 2004), while tortuosity can be lowered by deformation (Degruyter et al., 2010a). Incorporating the coupling between the textures and the magma properties is worthy of future study.

## Acknowledgments

WD was supported by the Swiss National Science Foundation Grant No. PBGEP2-131251, and MM by NSF EAR 1049662. We thank Sebatian Mueller for providing permeability data and two reviewers for their comments that improved this paper.

## References

Bernard, M.L., Zamora, M., Geraud, Y., Boudon, G., 2007. Transport properties of pyroclastic rocks from Montagne Pelée volcano (Martinique, Lesser Antilles). J. Geophys. Res. 112, B05205. doi:10.1029/2006JB004385.

Blower, J.D., 2001. Factors controlling permeability-porosity relationships in magma. Bull. Volcanol. 63, 497–504. doi:10.1007/s004450100172.

Blundy, J., Cashman, K., 2005. Rapid decompression-driven crystallization recorded by melt inclusions from Mount St. Helens volcano. Geology 33, 793–796. doi:10.1130/G21668.1.

Burgisser, A., Gardner, J.E., 2004. Experimental constraints on degassing and permeability in volcanic conduit flow. Bull. Volcanol. 67, 42–56. doi:10.1007/s00445–004–0359–5.

Burgisser, A., Poussineau, S., Arbaret, L., Druitt, T., Giachetti, T., Bourdier, J.L., 2010. Pre-explosive conduit conditions of the 1997 Vulcanian explosions at Soufrière Hills Volcano, Montserrat: I. pressure and vesicularity distributions. J. Volcanol. Geotherm. Res. 194, 27–41. doi:10.1016/j.jvolgeores.2010.04.008.

Carey, S., Sigurdsson, H., Gardner, J., Criswell, W., 1990. Variations in column height and magma discharge during the May 18, 1980 eruption of Mount St. Helens. J. Volcanol. Geotherm. Res. 43, 99–112. doi:10.1016/0377–0273(90)90047–J.

Clarke, A., Stephens, S., Teasdale, R., Sparks, R., Diller, K., 2007. Petrologic constraints on the decompression history of magma prior to Vulcanian explosions at the Soufrière Hills volcano, Montserrat. J. Volcanol. Geotherm. Res. 161, 261–274. doi:10.1016/j.jvolgeores.2006.11.007.

Cordonnier, B., Hess, K.U., Lavallee, Y., Dingwell, D.B., 2009. Rheological properties of dome lavas: Case study of Unzen volcano. Earth Planet. Sci. Lett. 279, 263–272. doi:10.1016/j.epsl.2009.01.014.

Costa, A., 2005. Viscosity of high crystal content melts: dependence on solid fraction. Geophys. Res. Lett. 32, L22308. doi:10.1029/2005GL024303.

Couch, S., Sparks, R., Carroll, M., 2003. The kinetics of degassing-induced crystallization at Soufrière Hills Volcano, Montserrat. J. Petrol. 44, 1477–1502. doi:10.1093/petrology/44.8.1477.

Degruyter, W., Bachmann, O., Burgisser, A., 2010a. Controls on magma permeability in the volcanic conduit during the climactic phase of the Kos Plateau Tuff eruption (Aegean Arc). Bull. Volcanol. 72, 63–74. doi:10.1007/s00445–009–0302–x.

Degruyter, W., Burgisser, A., Bachmann, O., Malaspinas, O., 2010b. Synchrotron X-ray

microtomography and lattice Boltzmann simulations of gas flow through volcanic pumices. Geosphere 6, 470–481. doi:10.1130/GES00555.1.

Dingwell, D.B., 1996. Volcanic dilemma: Flow or blow? Science 273, 1054–1055. doi:10.1126/science.273.5278.1054.

Dobran, F., 1992. Nonequilibrium flow in volcanic conduits and application to the eruptions of Mt. St. Helens on May 18, 1980, and Vesuvius in AD 79. J. Volcanol. Geotherm. Res. 49, 285–311. doi:10.1016/0377–0273(92)90019–A.

Druitt, T., Young, S., Baptie, B., Bonadonna, C., Calder, E., Clarke, A., Cole, P., Harford, C., Herd, R., Luckett, R., Ryan, G., Voight, B., 2002. Episodes of cyclic vulcanian explosive activity with fountain collapse at Soufrire Hills Volcano, Montserrat, in: Druitt, T., Kokelaar, B. (Eds.), The eruption of Soufrire Hills Volcano, Montserrat, from 1995 to 1999, The Geological Society of London. pp. 281–306.

Dufek, J., Bergantz, G.W., 2005. Transient two-dimensional dynamics in the upper conduit of a rhyolitic eruption: A comparison of closure models for the granular stress. J. Volcanol. Geotherm. Res. 143, 113–132. doi:10.1016/j.jvolgeores.2004.09.013.

Eichelberger, J., Carrigan, C., Westrich, H., Price, R., 1986. Non-explosive silicic volcanism. Nature 323, 598–602. doi:10.1038/323598a0.

Ergun, S., 1952. Fluid flow through packed columns. Chem. Eng. Prog. 46, 89–94.

Forchheimer, P., 1901. Wasserbewegung durch boden. Z. Ver. Dtsch. Ing. 45, 1782–1788.

Formenti, Y., Druitt, T.H., 2003. Vesicle connectivity in pyroclasts and implications for the fluidization of fountain-collapse pyroclastic flows, Montserrat (West Indies). Earth Planet. Sci. Lett. 214, 561–574. doi:10.1016/S0012–821X(03)00386–8.

Fowler, A.C. Scheu, B., Lee, W., McGuinness, M., 2010. A theoretical model of the explosive fragmenation of vesicular magma. Proc. R. Soc. A 466, 731–752. doi: 10.1098/rspa.2009.0382.

447 Giachetti, T., Druitt, T., Burgisser, A., Arbaret, L., Galven, C., 2010. Bub-
448 ble nucleation, growth and coalescence during the 1997 Vulcanian explosions of
449 Soufrière Hills Volcano, Montserrat. J. Volcanol. Geotherm. Res. 193, 215–231.
450 doi:10.1016/j.jvolgeores.2010.04.001.

451 Gonnermann, H.M., Manga, M., 2003. Explosive volcanism may not be an inevitable con-
452 sequence of magma fragmentation. Nature 426, 432–435. doi:10.1038/nature02138.

453 Gonnermann, H.M., Manga, M., 2005. Nonequilibrium magma degassing: Results from
454 modeling of the ca. 1340 A.D. eruption of Mono Craters, California. Earth Planet. Sci.
455 Lett. 238, 1–16. doi:10.1016/j.epsl.2005.07.021.

456 Gonnermann, H.M., Manga, M., 2007. The fluid mechanics inside a volcano. Annu. Rev.
457 Fluid Mech. 39, 321–356. doi:10.1146/annurev.fluid.39.050905.110207.

458 Hess, K., Dingwell, D., 1996. Viscosities of hydrous leucogranitic melts: a non-Arrhenian
459 model. Am. Mineral. 81, 1297–1300.

460 Jaupart, C., Allegre, C., 1991. Gas content, eruption rate and instabilities of eruption
461 regime in silicic volcanoes. Earth Planet. Sci. Lett. 102, 413–429. doi:10.1016/0012–
462 821X(91)90032–D.

463 Klug, C., Cashman, K.V., 1994. Vesiculation of May 18, 1980 Mount St. Helens magma.
464 Geology 22, 468–472. doi:10.1130/0091–7613(1994)022¡0468:VOMMSH¿2.3.CO;2.

465 Klug, C., Cashman, K.V., 1996. Permeability development in vesiculating magmas: Impli-
466 cations for fragmentation. Bull. Volcanol. 58, 87–100. doi:10.1007/s004450050128.

467 Kozono, T., Koyaguchi, T., 2009a. Effects of relative motion between gas and liquid on 1-
468 dimensional steady flow in silicic volcanic conduits: 1. an analytical method. J. Volcanol.
469 Geotherm. Res. 180, 21–36. doi:10.1016/j.jvolgeores.2008.11.006.

470 Kozono, T., Koyaguchi, T., 2009b. Effects of relative motion between gas and liquid on
471 1-dimensional steady flow in silicic volcanic conduits: 2. origin of diversity of eruption
472 styles. J. Volcanol. Geotherm. Res. 180, 37–49. doi:10.1016/j.jvolgeores.2008.11.007.

Kozono, T., Koyaguchi, T., 2010. A simple formula for calculating porosity of magma in volcanic conduits during dome-forming eruptions. Earth Planets Space 62, 483–488. doi:10.5047/eps.2010.02.005.

Laumonier, M., Arbaret, L., Burgisser, A., Champallier, R., 2011. Porosity redistribution enhanced by strain localization in crystal-rich magmas. Geology 39, 715–718. doi:10.1130/G31803.1.

Le Pennec, J.L., Hermitte, D., Dana, I., Pezard, P., Coulon, C., Cocheme, J.J., Mulyadi, E., Ollagnier, F., Revest, C., 2001. Electrical conductivity and pore-space topology of Merapi lavas: Implications for the degassing of porphyritic andesite magmas. Geophys. Res. Lett. 28, 4283–4286. doi:10.1029/2001GL013401.

Bouvet de Maisonneuve, C., Bachmann, O., Burgisser, A., 2009. Characterization of juvenile pyroclasts from the Kos Plateau Tuff (Aegean Arc): insights into the eruptive dynamics of a rhyolitic caldera-forming eruption. Bull. Volcanol. 71, 643–658. doi:10.1007/s00445–008–0250–x.

Massol, H., Koyaguchi, T., 2005. The effect of magma flow on nucleation of gas bubbles in a volcanic conduit. J. Volcanol. Geotherm. Res. 143, 69–88. doi:10.1016/j.jvolgeores.2004.09.011.

Melnik, O., Barmin, A.A., Sparks, R.S.J., 2005. Dynamics of magma flow inside volcanic conduits with bubble overpressure buildup and gas loss through permeable magma. J. Volcanol. Geotherm. Res. 143, 53–68. doi:10.1016/j.jvolgeores.2004.09.010.

Melnik, O., Sparks, R., 1999. Nonlinear dynamics of lava dome extrusion. Nature 402, 37–41. doi:10.1038/46950.

Melnik, O., Sparks, R.S.J., 2002a. Dynamics of magma ascent and lava extrusion at Soufrière Hills Volcano, Montserrat, in: Druitt, T., Kokelaar, B. (Eds.), The eruption of Soufrière Hills Volcano, Montserrat, from 1995 to 1999, The Geological Society of London. pp. 153–171.

Melnik, O., Sparks, R.S.J., 2002b. Modelling of conduit flow dynamics during explosive activity at Soufrire Hills Volcano, Montserrat, in: Druitt, T., Kokelaar, B. (Eds.), The eruption of Soufrire Hills Volcano, Montserrat, from 1995 to 1999, The Geological Society of London. pp. 307–317.

Melnik, O.E., Blundy, J.D., Rust, A., Muir, D.D., 2011. Subvolcanic plumbing systems imaged through crystal size distributions. Geology 39, 403406. doi:10.1130/G31691.1.

Michaut, C., Bercovici, D., Sparks, R.S.J., 2009. Ascent and compaction of gas rich magma and the effects of hysteretic permeability. Earth Planet. Sci. Lett. 282, 258–267. doi:10.1016/j.epsl.2009.03.026.

de' Michieli Vitturi, M., Clarke, A., Neri, A., Voight, B., 2010. Transient effects of magma ascent dynamics along a geometrically variable dome-feeding conduit. Earth Planet. Sci. Lett. 295, 541–553. doi:10.1016/j.epsl.2010.04.029.

Moore, J., Lipman, P., Swanson, D., Alpha, T.R., 1981. Growth of lava domes in the crater, June 1980-January 1981, in: Lipman, P.W.and Mullineaux, D. (Ed.), The 1980 eruptions of Mount St. Helens, Washington, US Gov. Printing Office, Washington, DC, USA. pp. 541–547.

Mueller, S., Melnik, O., Spieler, O., Scheu, B., Dingwell, D.B., 2005. Permeability and degassing of dome lavas undergoing rapid decompression: An experimental determination. Bull. Volcanol. 67, 526–538. doi:10.1007/s00445–004–0392–4.

Namiki, A., Manga, M., 2008. Transition between fragmentation and permeable outgassing of low viscosity magmas. J. Volcanol. Geotherm. Res. 169, 48–60. doi:10.1016/j.jvolgeores.2007.07.020.

Okumura, S., Nakamura, M., Tsuchiyama, A., 2006. Shear-induced bubble coalescence in rhyolitic melts with low vesicularity. Geophys. Res. Lett. 33, L20316, doi:10.1029/2006GL027347.

524 Papale, P., 1999. Strain-induced magma fragmentation in explosive eruptions. Nature 397,
525 425–428. doi:10.1038/17109.

526 Polacci, M., Baker, D.R., Mancini, L., Tromba, G., Zanini, F., 2006. Three-dimensional
527 investigation of volcanic textures by X-ray microtomography and implications for conduit
528 processes. Geophys. Res. Lett. 33, L13312. doi:10.1029/2006GL026241.

529 Ruprecht, P., Bachmann, O., 2010. Pre-eruptive reheating during magma mixing at Quizapu
530 volcano and the implications for the explosiveness of silicic arc volcanoes. Geology 38, 919–
531 922. doi:10.1130/G31110.1.

532 Rust, A.C., Cashman, K.V., 2004. Permeability of vesicular silicic magma: inertial and
533 hysteresis effects. Earth Planet. Sci. Lett. 228, 93–107. doi:10.1016/j.epsl.2004.09.025.

534 Saar, M.O., Manga, M., 1999. Permeability-porosity relationship in vesicular basalts. Geo-
535 phys. Res. Lett. 26, 111–114. doi:10.1029/1998GL900256.

536 Sable, J., Houghton, B., Del Carlo, P., Coltelli, M., 2006. Changing conditions of magma
537 ascent and fragmentation during the Etna 122 BC basaltic Plinian eruption: Evidence from
538 clast microtextures. Bull. Volcanol. 158, 333–354. doi:10.1016/j.jvolgeores.2006.07.006.

539 Shampine, L.F., Reichelt, M.W., 1997. The Matlab ODE suite. SIAM J. Sci. Stat. Comp.
540 18, 1–22. doi:10.1137/S1064827594276424.

541 Slezin, Y.B., 1983. The dynamics of dispersion regime in volcanic eruptions: 1. Theoretical
542 description of magma movement through volcanic conduit (in Russian). Vulkanol Sejsmol
543 5, 9–17.

544 Slezin, Y.B., 2003. The mechanism of volcanic eruptions (a steady state approach). J.
545 Volcanol. Geotherm. Res. 122, 7–50. doi:10.1016/S0377–0273(02)00464–X.

546 Stasiuk, M., Barclay, J., Caroll, M., Jaupart, C., Ratt, J., Sparks, R., Tait, S., 1996. De-
547 gassing during magma ascent in the Mule Creek vent (USA). Bull. Volcanol. 58, 117–130.
548 doi:10.1007/s004450050130.

549 Takeuchi, S., Nakashima, S., Akihiko Tomiya, A., 2008. Permeability measurements of
550 natural and experimental volcanic materials with a simple permeameter: Toward an un-
551 derstanding of magmatic degassing processes. J. Volcanol. Geotherm. Res. 177, 329–339.
552 doi:10.1016/j.jvolgeores.2008.05.010.

553 Takeuchi, S., Tomiya, A., Shinohara, H., 2009. Degassing conditions for permeable silicic
554 magmas: Implications from decompression experiments with constant rates. Earth Planet.
555 Sci. Lett. 283, 101–110. doi:10.1016/j.epsl.2009.04.001.

556 Toramaru, A., 2006. BND (bubble number density) decompression rate meter
557 for explosive volcanic eruptions. J. Volcanol. Geotherm. Res. 154, 303–316.
558 doi:10.1016/j.jvolgeores.2006.03.027.

559 Tuffen, H., Dingwell, D., Pinkerton, H., 2003. Repeated fracture and healing of silicic magma
560 generate flow banding and earthquakes? Geology 31, 1089–1092. doi:10.1130/G19777.1.

561 Webb, S.L., Dingwell, D.B., 1990. Non-Newtonian rheology of igneous melts at high stresses
562 and strain rates: Experimental results from rhyolite, andesite, basalt, and nephelinite. J.
563 Geophys. Res. 95, 15695–15701. doi:10.1029/JB095iB10p15695.

564 Woods, A.W., Koyaguchi, T., 1994. Transitions between explosive and effusive eruptions of
565 silicic magmas. Nature 370, 641–644. doi:10.1038/370641a0.

566 Wright, H.M.N., Cashman, K.V., Gottesfeld, E.H., Roberts, J.J., 2009. Pore structure of
567 volcanic clasts: Measurements of permeability and electrical conductivity. Earth Planet.
568 Sci. Lett. 280, 93–104. doi:10.1029/2006GL027224.

569 Wright, H.M.N., Roberts, J.J., Cashman, K.V., 2006. Permeability of anisotropic tube
570 pumice: Model calculations and measurements. Geophys. Res. Lett. 33, L17316.
571 doi:10.1016/j.epsl.2009.01.023.

572 Yokoyama, T., Takeuchi, S., 2009. Porosimetry of vesicular volcanic products by a water-
573 expulsion method and the relationship of pore characteristics to permeability. J. Geophys.
574 Res. 114, B02201. doi:10.1029/2008JB005758.

575 Yoshida, S., Koyaguchi, T., 1999. A new regime of volcanic eruption due to the relative mo-
576 tion between liquid and gas. J. Volcanol. Geotherm. Res. 89, 303–315. doi:10.1016/S0377–
577 0273(99)00005–0.

578 Zhang, Y., 1999. A criterion for the fragmentation of bubbly magma based on brittle failure
579 theory. Nature 402, 648–650. doi:10.1038/45210.

Table 1: Parameter space explored with the conduit model.

| parameter | symbol | value | | unit |
|---|---|---|---|---|
| **constants** | | | | |
| specific gas constant of water | $R$ | 461.4 | | J kg$^{-1}$ K$^{-1}$ |
| Einstein constant | $B$ | 2.5 | | |
| constants equation (13) | $c_1$ | 0.9995 | | |
| | $c_2$ | 0.4 | | |
| | $c_3$ | 1 | | |
| ash particle size | $r_a$ | $1 \times 10^{-3}$ | | m |
| gas-wall drag coefficient | $\lambda_w$ | 0.03 | | |
| gas-ash particle drag coefficient | $C_D$ | 0.8 | | |
| **textures** | | | | |
| bubble number density | $N_d$ | $10^8$–$10^{16}$ | | m$^{-3}$ |
| tortuosity factor | $m$ | 1–10 | | |
| friction coefficient | $f_0$ | $10^{-4}$–$10^2$ | | |
| throat-bubble ratio | $f_{tb}$ | 0.05 – 0.5 | | |
| **conduit geometry** | | MSH 1980 | SHV 1997 | |
| length | $L$ | 5291 | 5000 | m |
| radius | $r_c$ | 30 | 22.5 | m |
| **magma properties** | | MSH 1980 | SHV 1997 | |
| density | $\rho_m$ | 2500 | 2450 | kg m$^{-3}$ |
| temperature | $T$ | 1159 | 1123 | K |
| volatile content | $c_0$ | 4.6 | 4.6 | wt.% |
| crystal content | $\chi_0$ | 0.4 | 0.45 | |
| pressure | $P_0$ | 140 | 120 | MPa |

Table 2: Values and range of dimensionless parameters.

| parameter | symbol | value | |
|---|---|---|---|
| **fixed parameters** | | MSH 1980 | SHV 1997 |
| Reynolds number | Re | 6.69 | 0.27 |
| Froude number | Fr | 0.15 | 0.026 |
| Mach number | Ma | 0.0193 | 0.0033 |
| water content | $c_0$ | 0.046 | 0.046 |
| crystal content | $\chi_0$ | 0.4 | 0.45 |
| fragmentation gas volume fraction | $\phi_f$ | 0.8 | 0.8 |
| density ratio | $\delta$ | 0.1 | 0.1 |
| saturation water content at $P_0$ | $\sigma$ | 0.049 | 0.045 |
| ash/conduit size ratio | $a_r$ | $3.33 \times 10^{-5}$ | $4.44 \times 10^{-5}$ |
| **outgassing parameters** | | | |
| Stokes number | St | $10^{-6} - 10^{1}$ | |
| Forchheimer number | Fo | $10^{-3} - 10^{7}$ | |

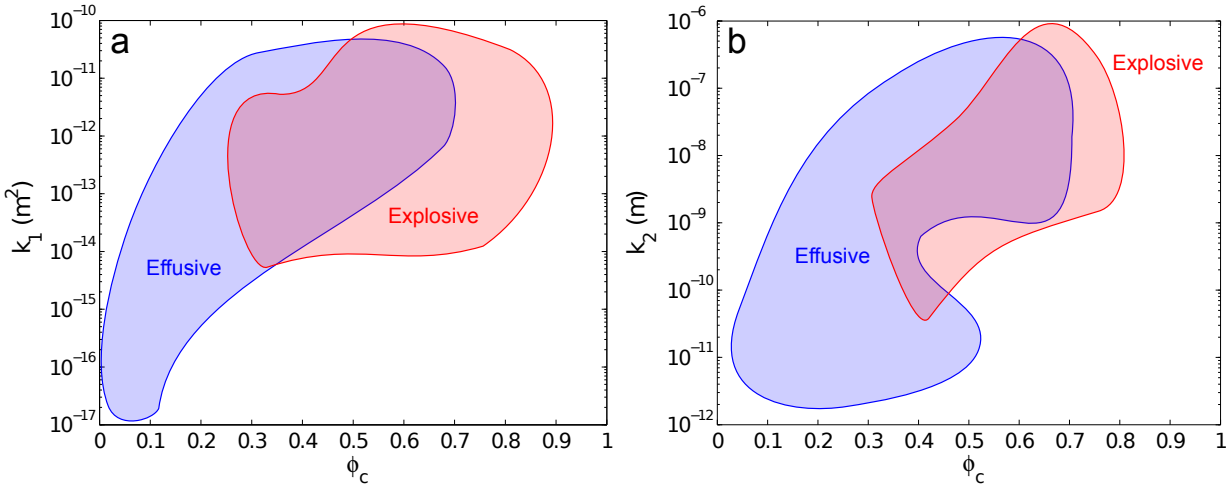


Figure 1: Summary of the relationship between of connected porosity $\phi_c$ and permeability. The blue area represents the spread in data collected on pyroclasts from effusive eruptions, the red area represents the data spread on pyroclasts from explosive eruptions for (a) Darcian permeability $k_1$ (Wright et al., 2009), and (b) inertial permeability $k_2$ (Rust and Cashman, 2004; Mueller et al., 2005; Takeuchi et al., 2008; Bouvet de Maisonneuve et al., 2009; Yokoyama and Takeuchi, 2009). Data from pyroclasts ejected by Vulcanian explosions are treated as effusive. Data are mostly from silica-rich pyroclasts, but also includes mafic products as porosity-permeability data does not appear to depend on composition.

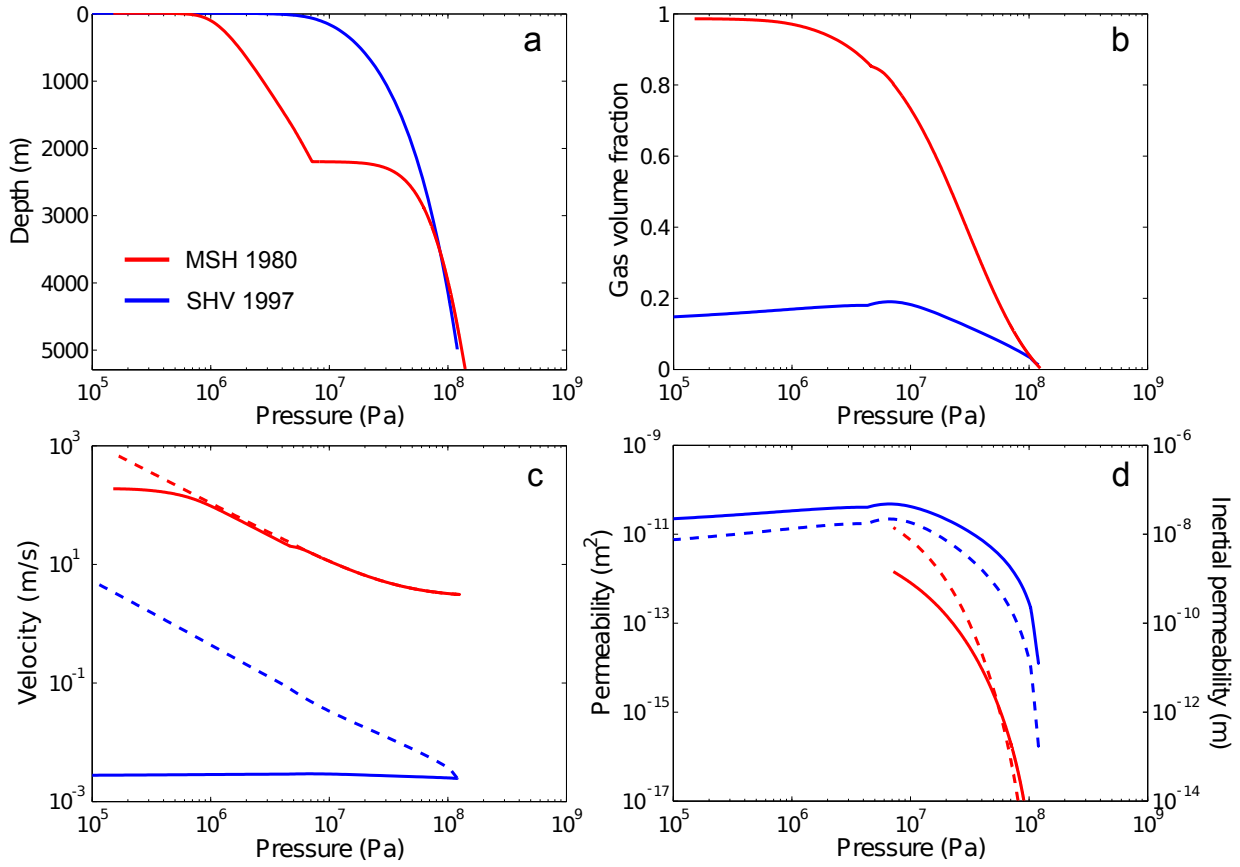


Figure 2: Illustrative solutions to the conduit model for MSH 1980 conditions with $N_d = 10^{15}$ m$^{-3}$, $m = 3.5$, $f_{tb} = 0.1$, $f_0 = 10$ (red) and SHV 1997 conditions with $N_d = 10^9$ m$^{-3}$, $m = 2.2$, $f_{tb} = 0.3$, $f_0 = 10$ (blue) using a fragmentation criterion based on volume fraction. (a) depth versus pressure, (b) porosity versus pressure, (c) velocity versus pressure with the dashed curves indicating the gas velocity and the solid curves showing the magma velocity, and (d) the Darcian (solid curves) and the inertial permeability (dashed curves).

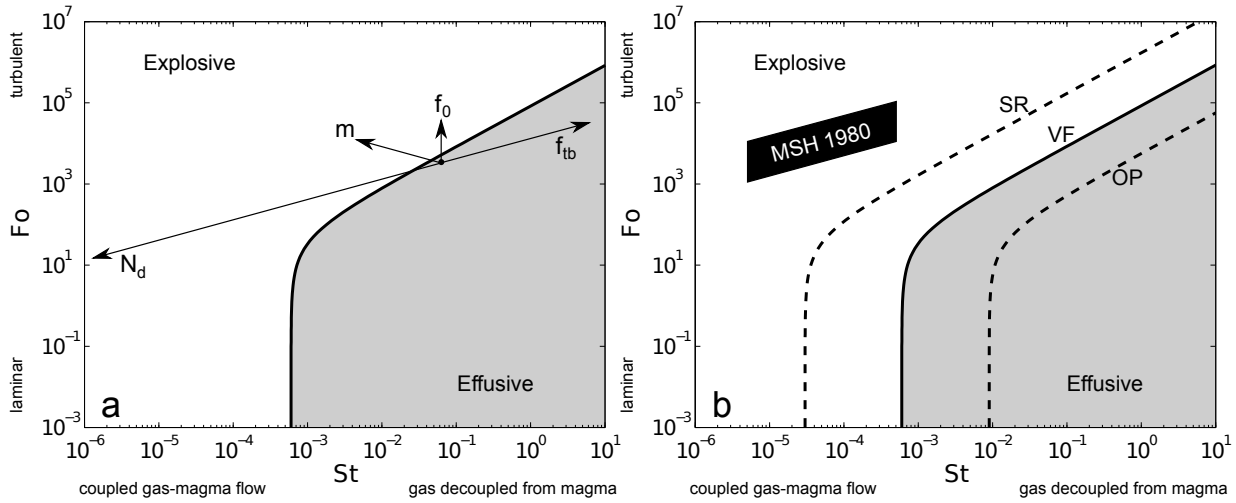


Figure 3: St-Fo map for the MSH 1980 magma properties and conduit geometry. The white area represents the explosive regime, and the grey area the effusive regime. (a) The arrows indicate how one travels on the map by increasing one of the textural properties starting from a randomly chosen point. The relative lengths of the arrows are determined by the range defined in Table 1. (b) The black area is defined by the textural properties found in the pyroclasts of the MSH 1980 eruption. It lies in the low St and high Fo region showing that the gas-magma flow was coupled and outgassing was turbulent. The dashed curves indicate the transition between effusive and explosive regimes for strain-rate fragmentation (SR) and overpressure fragmentation (OP), while the solid curve indicates fragmentation at a critical gas volume fraction (VF). See Appendix B for details on fragmentation criteria.

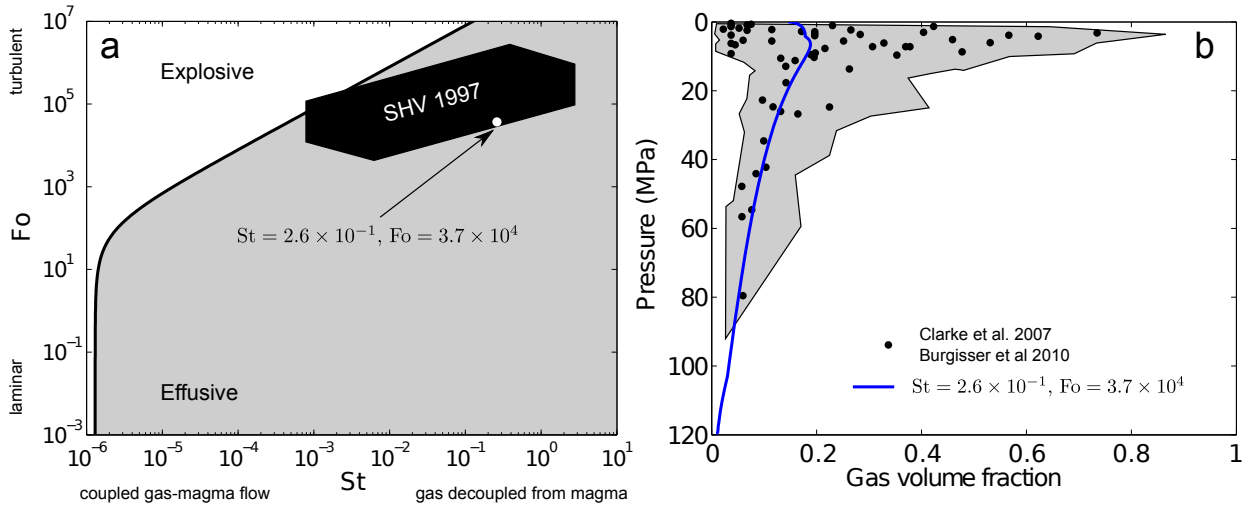


Figure 4: (a) St-Fo map for the SHV 1997 eruption conditions as determined from Monte Carlo simulations. The black area is defined by the textural properties found in the pyroclasts produced by the SHV 1997 eruptions. We can refine the black region to the white point by using the data points of pressure and gas volume fraction collected by Clarke et al. (2007) and Burgisser et al. (2010) in figure (b). The gray area in figure (b) represents the uncertainty in the model used by Burgisser et al. (2010) to obatin pre-explosive gas volume fraction. The blue line is the best fit of the model to this data for $P > 10$ MPa: $\mathrm{St} = 2.6 \times 10^{-1}$, $\mathrm{Fo} = 3.7 \times 10^{4}$,e.g. $N_d = 10^{9.5}$ m$^{-3}$, $f_{tb} = 10^{-0.5}$, $m = 2.1$, and $f_0 = 10$.

## Appendix A. Non-dimensionalization

We scale the equations of the conduit model to permit better interpretation of the results. The model parameters can be divided into three main groups: (i) conduit geometry $L$, $r_c$, (ii) magma properties $P_0$, $T$, $c_0$, $\phi_f$, $\rho_m$, $\chi_0$, and (iii) magma textures $f_{tb}$, $f_0$, $N_d$, $m$. From these parameters we define all other characteristic scales: a reference gas density

$$\rho_{g0} = \frac{P_0}{RT}, \tag{A.1}$$

a reference viscosity

$$\log \mu_0 = -3.545 + 0.833 \ln 100c_0 + \frac{9601 - 2368 \ln 100c_0}{T - (195.7 + 32.25 \ln 100c_0)} \tag{A.2}$$

$$\theta_0 = \left\{ 1 - c_1 \mathrm{erf}\left( \frac{\sqrt{\pi}}{2} \chi_0 \left[ 1 + \frac{c_2}{(1-\chi_0)^{c_3}} \right] \right) \right\}^{-B/c_1} \tag{A.3}$$

$$\mu_{l0} = \mu_0 \theta_0 \tag{A.4}$$

a reference mass and volume flux

$$q_0 = \frac{P_0}{L} \frac{\rho_m r_c^2}{8\mu_{l0}}, \quad U_0 = \frac{q_0}{\rho_m}, \tag{A.5}$$

and the reference Darcian and inertial permeability

$$k_{10} = \frac{\phi_f^m (f_{tb} r_{b0})^2}{8}, \tag{A.6}$$

$$k_{20} = \frac{(f_{tb} r_{b0}) \phi_f^{\frac{1+3m}{2}}}{f_0}, \tag{A.7}$$

with

$$r_{b0} = \left( \frac{\phi_f}{\frac{4\pi}{3} N_d (1 - \phi_f)} \right)^{1/3}. \tag{A.8}$$

We then define the dimensionless quantities

$$u'_m = \frac{u_m}{U_0},\ u'_g = \frac{u_g}{U_0},\ \rho'_g = \frac{\rho_g}{\rho_{g0}},\ \mu'_m = \frac{\mu_{l0}}{\mu_0},\ k'_1 = \frac{k_1}{k_{10}},\ k'_2 = \frac{k_2}{k_{20}},\ q' = \frac{q}{q_0} \tag{A.9}$$

Substituting these in the conservation equations gives

$$u'_m = \frac{1-n}{1-\phi} q' \tag{A.10}$$

$$\rho'_g u'_g = \frac{1}{\delta}\frac{n}{\phi} q' \tag{A.11}$$

$$u'_m \frac{du'_m}{dz'} = -\frac{3}{4}\delta \frac{1}{\mathrm{Ma}^2}\frac{dP'}{dz'} - \frac{1}{\mathrm{Fr}^2} + \frac{F'_{mg}}{1-\phi} - \frac{F'_{mw}}{1-\phi} \tag{A.12}$$

$$\rho'_g u'_g \frac{du'_g}{dz'} = -\frac{3}{4}\frac{1}{\mathrm{Ma}^2}\frac{dP'}{dz'} - \frac{1}{\mathrm{Fr}^2}\rho'_g - \frac{1}{\delta}\frac{F'_{mg}}{\phi} - \frac{F'_{gw}}{\phi} \tag{A.13}$$

$$F'_{mg} = \begin{cases} \frac{1}{\mathrm{St}}\left(1 + \mathrm{Fo}\,\frac{k'_1}{k'_2}\rho'_g |u'_g - u'_m|\right)\frac{\phi(1-\phi)}{k'_1}(u'_g - u'_m) & \phi \le \phi_t \\ \left(\frac{1}{k'_1 \mathrm{St}}\left(1 + \mathrm{Fo}\,\frac{k'_1}{k'_2}\rho'_g |u'_g - u'_m|\right)\right)^{1-t}\left(\frac{3}{8}\frac{1}{a_r} C_D \rho'_g |u'_g - u'_m|\right)^t \phi(1-\phi)(u'_g - u'_m) & \phi_t < \phi \le \phi_f \\ \frac{3}{8}\frac{1}{a_r} C_D \rho'_g \phi(1-\phi)|u'_g - u'_m|(u'_g - u'_m) & \phi > \phi_f \end{cases} \tag{A.14}$$

$$F'_{mw} = \begin{cases} \frac{8\mu'_m u'_m}{\mathrm{Re}} & \phi \le \phi_f \\ 0 & \phi > \phi_f \end{cases} \tag{A.15}$$

$$F'_{gw} = \begin{cases} 0 & \phi \le \phi_f \\ \frac{\lambda_w}{4}\rho'_g u_g^{'2} & \phi > \phi_f \end{cases} \tag{A.16}$$

$$n = \frac{c_0 - \sigma P'^{1/2}}{1 - \sigma P'^{1/2}} \quad (n \ge 0), \tag{A.17}$$

with Re the Reynolds number of the magma phase,

$$\mathrm{Re} = \frac{\rho_m r_c U_0}{\mu_{l0}}, \tag{A.18}$$

Ma the Mach number of the gas phase (water),

$$\mathrm{Ma} = \frac{U_0}{\sqrt{\frac{4}{3}RT}}, \tag{A.19}$$

Fr the Froude number,

$$\mathrm{Fr} = \frac{U_0}{\sqrt{g r_c}}, \tag{A.20}$$

$\delta$ the density ratio between the gas and the magma phase,

$$\delta = \frac{\rho_{g0}}{\rho_m}, \tag{A.21}$$

$\sigma$ the saturation water content at initial pressure $P_0$,

$$\sigma = sP_0^{1/2}, \tag{A.22}$$

and $a_r$ the ratio between the ash size and the conduit radius,

$$a_r = \frac{r_a}{r_c}. \tag{A.23}$$

St is the Stokes number, the ratio of the response time scale of the magma and the characteristic flow time of the gas

$$\mathrm{St} = \frac{\tau_V}{\tau_F} = \frac{\frac{\rho_m k_{10}}{\mu_g}}{\frac{r_c}{U_0}} \tag{A.24}$$

and Fo is the Forchheimer number the ratio of the inertial term and the viscous term in Forchheimer's equation

$$\mathrm{Fo} = \frac{\rho_{g0} k_{10} U_0}{k_{20} \mu_g}. \tag{A.25}$$

From this scaling analysis we find two parameters that are influenced by textures, St and Fo. When keeping the conduit geometry and magma properties constant only St and Fo will vary, while others remain constant (Table 2). Therefore, the textural control on the effusive-explosive transition can be projected onto a St-Fo plane. We create such a St-Fo map for two case studies by doing Monte Carlo simulations within the defined texture parameter space (Table 1).

## Appendix B. Fragmentation mechanisms

We investigate the effect of different fragmentation mechanisms on the results, using either a criterion based on (i) critical strain-rate, (ii) overpressure or (iii) volume fraction. The strain-rate criterion was defined by Dingwell (1996) and Papale (1999) as

$$\frac{du_m}{dz} > 0.01 \frac{G}{\mu_m}, \tag{B.1}$$

with $G = 10$ GPa. Note that we use the elongational strain-rate and not the shear-strain rate, which cannot be assessed by a one-dimensional model (Gonnermann and Manga, 2003). Overpressure cannot be directly calculated in our model as the pressure between both phases

is at equilibrium. However, we assume the overpressure can be quantified by the dynamic pressure induced by the interphase drag between the two phases

$$\frac{dP_\Delta}{dz} = F_{mg} \tag{B.2}$$

Integrating this equation along with the governing conservation equations gives us an estimate of the overpressure $P_\Delta$ in the bubble network. Following Zhang (1999), fragmentation occurs when

$$P_\Delta > \frac{2(1-\phi)}{(1+2\phi)} P_c \tag{B.3}$$

where we used $P_c = 100$ MPa (Webb and Dingwell, 1990). Our results show a shift in the transition curve (Figure 3b), but do not produce any qualitative difference in the results. These findings are in agreement with other studies comparing different fragmentation mechanisms (Melnik and Sparks, 2002b; Massol and Koyaguchi, 2005).